

Characterizing photon number statistics using conjugate optical homodyne detection

Bing Qi,^{1,2,*} Pavel Lougovski,^{1,†} and Brian P. Williams^{1,‡}

¹*Quantum Information Science Group, Computational Sciences and Engineering Division,
Oak Ridge National Laboratory, Oak Ridge, TN 37831-6418, USA*

²*Department of Physics and Astronomy, The University of Tennessee, Knoxville, TN 37996 - 1200, USA*

(Dated: February 9, 2017)

We study the problem of determining the photon number statistics of an unknown quantum state for a single-mode electromagnetic field using conjugate optical homodyne detection. By defining an observable Z as a sum of squared outputs of two homodyne detectors, we show that the photon number statistics can be recovered in repeated measurements of Z on an ensemble of identical input states without controlling the phase of an input signal or randomizing the phase of a local oscillator. We demonstrate how the expectation maximization algorithm and Bayesian inference can be utilized to facilitate the reconstruction. We also compare the performance of our detection method to a commonly used single photon detector in the case of a single-shot measurement. We illustrate our approach by conducting experiments to study the photon number distribution of a weak coherent and a thermal state source. ^a

PACS numbers: 42.50.-P; 42.50.Ar

I. INTRODUCTION

Single photon detector (SPD) is a workhorse of modern quantum optics experiments. It is commonly used to determine the number of photons in a given light pulse [1] in a single-shot measurement scenario. However, today's SPDs are expensive and have a limited photon number resolving ability. Alternatively, given a large ensemble of identical input states, optical homodyne detection (OHD) can be used to completely reconstruct the quantum state of the ensemble, including the photon number statistics. This method is known as the optical homodyne tomography [2, 3].

In OHD, a strong local oscillator (LO) is mixed with a very weak input signal at a beam splitter. The outputs of the beam splitter are strong enough to be detected by low cost, highly efficient photo-diodes working at room temperature. This makes OHD an appealing solution in practice. Note, the LO in OHD also functions as a mode selector: only the signals in the same spatiotemporal mode as the LO will be detected. This can be advantageous in certain applications such as, for example, quantum key distribution (QKD) [4–7], where the mode selecting function allows us to effectively sup-

press broadband background noise originating from the communication channel [8–10].

Given the LO is sufficiently strong, a DC-balanced homodyne detector measures quadrature X_θ of the input signal, where θ is the phase of the LO [11, 12]. To reconstruct the full quantum state, repeated measurements are required for all values of $\theta \in [0, 2\pi]$. Obviously, a crucial requirement for such a reconstruction scheme is that the phase of the input state is well known. However, in many applications, this requirement can not be easily satisfied. For example, in QKD, the signal measured at the receiver typically comes from a channel controlled by an adversary. In this case, we cannot make any assumptions about its phase. Fortunately, it has been shown that the photon number statistics of an input state with an unknown phase can still be fully recovered by using either one or two optical homodyne detectors, given the phase of the LO is uniformly randomized [13–16]. The phase randomization process can be implemented by using a phase modulator driven by a random pattern, as demonstrated in [17].

In this paper, we further develop the double homodyne detection scheme [16] and remove the requirement of LO phase randomization, thus simplifying its implementation. The basic idea is to define a new measurement observable Z as a sum of the squared outputs of the two homodyne detectors. In classical electrodynamics, the outputs of two conjugate homodyne detectors can be defined as the in-phase and out-of-phase components of an electromagnetic wave, so the observable Z defined above is proportional to the intensity (or the photon number) of the input signal. In quantum mechanics, canonically conjugate quadrature components of quantum optical fields do not commute with each other and, thus, they cannot be determined simultaneously and noiselessly due to Heisenberg's uncertainty principle. Nevertheless, a single-shot measurement of Z can still provide a partial information about the photon number of the input state.

* qib1@ornl.gov

† lougovskip@ornl.gov

‡ williamsbp@ornl.gov

^a This manuscript has been authored by UT-Battelle, LLC under Contract No. DE-AC05-00OR22725 with the U.S. Department of Energy. The United States Government retains and the publisher, by accepting the article for publication, acknowledges that the United States Government retains a non-exclusive, paid-up, irrevocable, world-wide license to publish or reproduce the published form of this manuscript, or allow others to do so, for United States Government purposes. The Department of Energy will provide public access to these results of federally sponsored research in accordance with the DOE Public Access Plan (<http://energy.gov/downloads/doe-public-access-plan>).

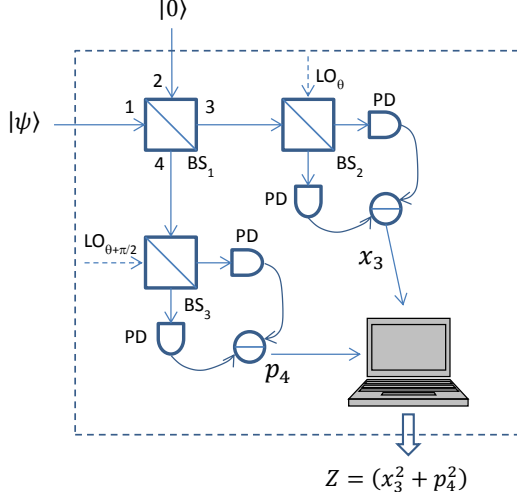


FIG. 1: Characterizing photon number statistics using conjugate optical homodyne detection. BS: symmetric beam splitter; PD: photo detector; LO: local oscillator.

By repeating the Z measurement on a large ensemble of identical states, the photon number statistics can be determined.

This paper is organized as follows: in Sec.II, we present theoretical analysis of the proposed scheme. In Sec.III, we present experimental results based on a weak coherent source and a thermal source. Finally, we conclude this paper with a brief discussion in Sec.IV.

II. THEORY

In this Section, we assume perfect homodyne detectors with unity efficiency. We will discuss the case of non-unity detection efficiency in Sec.III.

A. Conjugate homodyne detection

The basic setup of a conjugate homodyne detection system is shown in Fig.1. An unknown quantum state $|\psi\rangle$ is split by a symmetric beam splitter (BS₁ in Fig.1). One output state of the beam splitter (output 3 in Fig.1) is measured by an optical homodyne detector with a local oscillator (LO) phase θ ; the other output state (output 4 in Fig.1) is measured by an optical homodyne detector with an LO phase $\theta + \pi/2$. The common phase θ is defined using the phase of the input state as a reference. Provided that the input state has an unknown phase which may change from pulse to pulse, we have no control of θ (i.e. θ is a random variable with an unknown distribution). On the other hand, since the two LOs can be generated from the same laser, the $\pi/2$ phase difference between them can be well controlled.

Given the LOs are sufficiently strong, the outputs of the two homodyne detectors are quadrature components of mode 3 ($x_{3,\theta}$) and mode 4 ($x_{4,\theta+\pi/2}$). For simplicity, we use x_3 and p_4 to represent $x_{3,\theta}$ and $x_{4,\theta+\pi/2}$ in the rest of the paper.

We define a new parameter z as

$$z = x_3^2 + p_4^2 \quad (1)$$

as an estimate of the photon number of the input state $|\psi\rangle$. Intuitively, z is proportional to the intensity of the input light in classical electrodynamics. So, we expect a single measurement of z will provide some photon number information.

In quantum optics, the measurement processes of the two homodyne detectors are represented by operators \hat{X}_3 and \hat{P}_4 , which are defined in terms of photon annihilation operator \hat{a} and photon creation operator \hat{a}^\dagger as

$$\hat{X}_3 = \frac{1}{\sqrt{2}} [\hat{a}_3^\dagger \exp(i\theta) + \hat{a}_3 \exp(-i\theta)], \quad (2)$$

$$\hat{P}_4 = \frac{i}{\sqrt{2}} [\hat{a}_4^\dagger \exp(i\theta) - \hat{a}_4 \exp(-i\theta)]. \quad (3)$$

We define an operator \hat{Z} corresponding to z as

$$\hat{Z} = \hat{X}_3^2 + \hat{P}_4^2. \quad (4)$$

Using the transformation relations of a symmetric beam splitter [18]

$$\hat{a}_3 = \frac{1}{\sqrt{2}}(\hat{a}_1 + \hat{a}_2), \quad (5)$$

$$\hat{a}_4 = \frac{1}{\sqrt{2}}(\hat{a}_1 - \hat{a}_2), \quad (6)$$

and the commutation relation

$$[\hat{a}_j, \hat{a}_j^\dagger] = 1, \quad (7)$$

(where $j=1,2,3,4$), it can be shown that

$$\hat{Z} = \hat{n}_1 + \hat{n}_2 + \hat{a}_1^\dagger \hat{a}_2^\dagger e^{i2\theta} + \hat{a}_1 \hat{a}_2 e^{-i2\theta} + 1 \quad (8)$$

where $\hat{n}_1 = \hat{a}_1^\dagger \hat{a}_1$ and $\hat{n}_2 = \hat{a}_2^\dagger \hat{a}_2$ are photon number operators of mode 1 and 2. Obviously, \hat{Z} is a Hermitian operator. Thus, it is a valid observable.

Expectation value of \hat{Z}

As shown in Fig.1, the joint input state of mode 1 and 2 is given by $|\psi_1 0_2\rangle$. From Eq.(8), the expectation value of \hat{Z} can be determined to be

$$\langle \hat{Z} \rangle = \langle \psi_1 0_2 | \hat{Z} | \psi_1 0_2 \rangle = \langle n_1 \rangle + 1, \quad (9)$$

where $\langle n_1 \rangle$ is the expected photon number of the input quantum state. The constant 1 on the RHS of Eq.(9) can be interpreted as the vacuum noise contribution from the

first beam splitter [19]. Eq.(9) shows that the average photon number of the input state can be estimated by subtracting 1 from the mean value of the measured z .

Variance of \hat{Z}

The variance of \hat{Z} is given by

$$\langle \Delta Z^2 \rangle = \langle (\hat{Z} - \langle \hat{Z} \rangle)^2 \rangle = \langle \hat{Z}^2 \rangle - \langle \hat{Z} \rangle^2. \quad (10)$$

From Eq.(8), it is straightforward to show

$$\langle \hat{Z}^2 \rangle = \langle \hat{n}_1^2 \rangle + 3\langle \hat{n}_1 \rangle + 2. \quad (11)$$

Using Eq.(9)-Eq.(11), we obtain

$$\langle \Delta Z^2 \rangle = \langle \Delta n_1^2 \rangle + \langle n_1 \rangle + 1, \quad (12)$$

where $\langle \Delta n_1^2 \rangle = \langle \hat{n}_1^2 \rangle - \langle n_1 \rangle^2$ is the variance of photon number distribution of the input state. Clearly, the additional noise of the proposed scheme is $\langle n_1 \rangle + 1$.

Second-order correlation function $g^{(2)}(0)$

The single-time second-order correlation function $g^{(2)}(0)$ is an important parameter to characterize a photon source [20]. In the case of a single homodyne detector with a phase randomized LO, it has been shown that $g^{(2)}(0)$ can be determined from the measurement statistics [21]. Here, we show that $g^{(2)}(0)$ can be conveniently calculated from the statistics of Z measurement.

As defined in [20]

$$g^{(2)}(0) = \frac{\langle \hat{a}_1^\dagger \hat{a}_1^\dagger \hat{a}_1 \hat{a}_1 \rangle}{\langle \hat{a}_1^\dagger \hat{a}_1 \rangle^2}. \quad (13)$$

Using Eq.(7), the numerator on the RHS of Eq.(13) can be written as $\langle \hat{a}_1^\dagger \hat{a}_1^\dagger \hat{a}_1 \hat{a}_1 \rangle = \langle \hat{a}_1^\dagger \hat{a}_1 \hat{a}_1^\dagger \hat{a}_1 - \hat{a}_1^\dagger \hat{a}_1 \rangle = \langle \hat{n}_1^2 \rangle - \langle \hat{n}_1 \rangle$. Using Eq.(9) and Eq.(11), we have

$$\langle \hat{a}_1^\dagger \hat{a}_1^\dagger \hat{a}_1 \hat{a}_1 \rangle = \langle \hat{Z}^2 \rangle - 4\langle \hat{Z} \rangle + 2. \quad (14)$$

From Eq.(9), the denominator on the RHS of Eq.(13) is simply $(\langle \hat{Z} \rangle - 1)^2$. Finally, we have

$$g^{(2)}(0) = \frac{\langle \hat{Z}^2 \rangle - 4\langle \hat{Z} \rangle + 2}{(\langle \hat{Z} \rangle - 1)^2}. \quad (15)$$

Probability distribution of \hat{Z}

Now we determine the probability distribution $P_Z(z)$ given an arbitrary input state described by the density matrix ρ .

The joint probability distribution of quadrature components x_3 and p_4 has been derived in [16] as

$$P_{X_3, P_4}(x_3, p_4) = \frac{1}{\pi} \sum_{m, n=0}^{\infty} \rho_{mn} \frac{\exp[i(n-m)\theta]}{(m!n!)^{1/2}} \times (x_3 - ip_4)^m (x_3 + ip_4)^n \exp[-(x_3^2 + p_4^2)]. \quad (16)$$

The data pair (x_3, p_4) can be interpreted as the Cartesian coordinates of a point, which relates to the Polar

Coordinates (r, ϕ) by $x_3 = r \cos \phi$ and $p_4 = r \sin \phi$. The marginal distribution of r is given by

$$P_R(r) = \int_0^{2\pi} P_{X_3, P_4}(r \cos \phi, r \sin \phi) d\phi. \quad (17)$$

Note the term $(x_3 - ip_4)^m (x_3 + ip_4)^n$ on the RHS of Eq.(16) is transformed into $r^{2n} \exp[i(n-m)\phi]$ in the Polar Coordinates. Obviously, only terms with $n = m$ have non-zero contribution in (17). It is straightforward to show

$$P_R(r) = 2 \exp(-r^2) \sum_{n=0}^{\infty} \frac{\rho_{nn}}{n!} r^{2n+1}. \quad (18)$$

Since the measured observable $z = r^2$, the probability distribution $P_Z(z)$ can be determined from Eq.(18) as

$$P_Z(z) = \exp(-z) \sum_{n=0}^{\infty} \frac{\rho_{nn}}{n!} z^n. \quad (19)$$

Eq.(19) is the main result of this paper, which gives the relation between the probability distribution of the measured observable z and the photon number distribution ρ_{nn} of the input state. Given a large number of identical copies of the input state, the photon number distribution can be retrieved from the measurement results precisely. Note $P_Z(z)$ is only dependent on the diagonal terms of the input state, a feature we would expect from a “phase-insensitive” photon detector. Experimentally, Eq.(19) implies that the photon number statistics can be determined without controlling (or randomizing) the phase of the LO.

Next, we will conduct numerical simulations to quantify the performance of the proposed scheme in different applications.

B. Single-shot measurement

Can we use the proposed measurement scheme to determine the photon number of the input state in a single-shot measurement?

Given the input state is a Fock state $\rho = |n\rangle\langle n|$, the likelihood of a measurement output of z can be determined from (19) as

$$P_Z(z|n) = \exp(-z) \frac{z^n}{n!}. \quad (20)$$

Using Bayes' rule the likelihood of n given the measurement output z is

$$P_Z(n|z) = \frac{P_Z(z|n)P(n)}{P(z)} = \exp(-z) \frac{z^n}{n!}, \quad (21)$$

where we have assumed that the prior $P(n)$ is a uniform distribution for $n=0,1,2,\dots$

The distribution in Eq.(21) is the Poisson distribution, which quantifies the uncertainty of the photon number n

after a single measurement of z . This shows that our measurement scheme is intrinsically noisy. The measurement variance can be determined from Eq.(21) as

$$\sigma = \langle \Delta n^2 \rangle = z. \quad (22)$$

Next, we evaluate the performance of the proposed scheme as a threshold SPD which discriminates vacuum state from other Fock states. The discrimination strategy is to choose a threshold value $T \in [0, \infty)$. The detector reports a detection event only when the measurement result z is larger than T .

Two important parameters of a threshold SPD are detection efficiency and dark count probability. The detection efficiency η is defined as the conditional probability that the detector reports a click given the input is a single photon Fock state. The dark count probability D is defined as the conditional probability that the detector reports a click given the input is vacuum state. From Eq.(20), these two parameters can be determined by

$$\eta = \int_T^\infty P_Z(z|1)dz \quad (23)$$

$$D = \int_T^\infty P_Z(z|0)dz \quad (24)$$

Fig.2 shows the simulation results of η and D as a function of the threshold value T . By choosing the right threshold value, we can either achieve a high detection efficiency or a low dark count. Unfortunately, we cannot have both at the same time. Similar conclusions had been drawn in previous studies based on the single homodyne detection scheme [22]. In Fig.2, we also present the ratio $R = \eta/D$, which is an important figure of merit in applications like QKD. A state-of-the-art SPD can provide a R-value as high as 10^8 [1]. In comparison, the R-value of the proposed scheme is less than 10 in the region with a reasonable detection efficiency.

In a brief summary, while the conjugate homodyne detection scheme can provide some photon number information of the input state in a single-shot measurement, its performance is inferior to a state-of-the-art SPD.

C. Repeated measurements

Given a sequence of M independent measurements of Z , denoted as $\{z_i\} = z_1, \dots, z_M$, we would like to infer the underlying photon number statistics given by the distribution $p(n) = \rho_{nn}$ for $n = 0, 1, \dots, N_{max}$. The observed data statistics can be described in terms of a mixture model of $N_{max} + 1$ gamma distributions $\text{Gamma}(n+1, 1)$ with mixing coefficients given by the photon number distribution $p(n)$. In this model the conditional probability of observing an outcome $Z_k = z_k$ given the mixture component $p(n_k)$ reads,

$$p(Z_k = z_k | \{p(n_k)\}, n_k) = p(n_k) \frac{\exp(-z_k) z_k^{n_k}}{n_k!}. \quad (25)$$

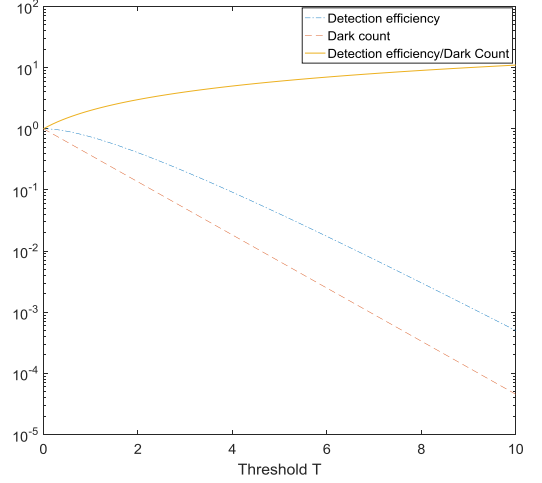


FIG. 2: (Color Online) Simulation results of detection efficiency η (Dash-dot line), dark count probability D (Dashed line), and the ratio $R = \eta/D$ (Solid line).

The complete data likelihood function \mathcal{L}_c for the entire measurement sequence can be written as,

$$\mathcal{L}_c = \prod_{k=1}^M p(Z_k = z_k | \{p(n)\}, n_k). \quad (26)$$

Here, $p(n), n = 0, \dots, N_{max}$ are the unknown parameters (Fock state probabilities) we wish to infer and n_1, \dots, n_M are random variables, each in range $[0, N_{max}]$, that determine which mixture component $n_i \in [0, N_{max}]$ has generated an outcome z_i . Have we known the values of n_1, \dots, n_M then we could use the maximum-likelihood estimation (MLE) based on \mathcal{L}_c to infer the most likely values of the parameters $p(n)$. Unfortunately the variables $n_i, i = 1, M$ are unobserved (latent). Therefore, in order to use MLE we first need to marginalize the complete data likelihood \mathcal{L}_c over the latent variables. The resulting marginal likelihood of the observed data reads,

$$\mathcal{L} = \prod_{k=1}^M \sum_{n_k=0}^{N_{max}} p(Z_k = z_k | \{p(n)\}, n_k), \quad (27)$$

where we used the following convention,

$$\prod_{k=1}^M \sum_{n_k=0}^{N_{max}} = \sum_{n_1=0}^{N_{max}} \cdots \sum_{n_M=0}^{N_{max}}. \quad (28)$$

In principle one now can try and maximize the function \mathcal{L} with respect to parameters $p(n)$, but in practice the complexity of this task will grow exponentially with the number of measurements M . Fortunately, there is a way to determine the maximum of $\log \mathcal{L}$ that avoids explicit maximization of \mathcal{L} . This method is widely used

for inference in mixture models and is called expectation-maximization (EM) algorithm [23]. Applicability of EM in the context of homodyne measurement of photon statistics has been advocated previously [24]. EM is an iterative procedure that uses the expected value of the complete data likelihood \mathcal{L}_c with respect to the latent random variables n_1, \dots, n_M as a maximization objective function for determining $p^t(n)$ – the t -th iteration estimate of the parameters $p(n)$. Here, is how it works:

First, set initial estimates of the parameters $p^0(n)$ to some values. We chose a uniform prior

$$p^0(n) = \frac{1}{N_{max} + 1}$$

as it is uninformative and easy to implement. Due to the multimodality of Eq. (27) the choice of prior will bias the EM reconstruction given below. It is an open problem to identify the best prior for this application¹. Next, repeat the following steps until convergence criteria are satisfied.

- At the t -th iteration, update probabilities $p(n_k|z_k, \{p^t(n)\})$ for all latent variables n_1, \dots, n_M using Bayes rule with $p^t(n)$ as a prior,

$$p(n_k|z_k, \{p^t(n)\}) = \frac{p(Z_k=z_k|\{p^t(n)\}, n_k)}{\sum_{n_k=0}^{N_{max}} p(Z_k=z_k|\{p^t(n)\}, n_k)}$$

- Calculate the expected value of the complete data log likelihood with respect to the updated distribution $p(n_k|z_k, \{p^t(n)\})$,

$$Q(\{p(n)\}|\{p^t(n)\}) = E_{\{n_k\}|\{z_k\}, \{p^t(n)\}}[\log \mathcal{L}_c] = \sum_{k=1}^M \sum_{j=0}^{N_{max}} p(j|z_k, \{p^t(n)\}) \log[p(Z_k = z_k|\{p(n)\}, j)]$$

- Find parameter values $\{p_{max}(n)\}$ that maximize $Q(\{p(n)\}|\{p^t(n)\})$ and set the next iteration estimates of photon number probabilities $\{p^{t+1}(n)\} = \{p_{max}(n)\}$. Note that the values of $\{p_{max}(n)\}$ can be calculated analytically,

$$p^{t+1}(n) = \frac{1}{M} \sum_{j=1}^M p(n|z_j, \{p^t(n)\}).$$

It can be shown [23] that iterative maximization of $Q(\{p(n)\}|\{p^t(n)\})$ also results in the maximization of the marginal likelihood \mathcal{L} in Eq.(27). Therefore, after a sufficient number of iterations t_s our MLE estimator of the photon number statistics is given by the distribution $\{p^{t_s}(n)\}$.

¹ In principal, one can choose any set of positive real numbers such that $\sum_{n=0}^{N_{max}} p^0(n) = 1$.

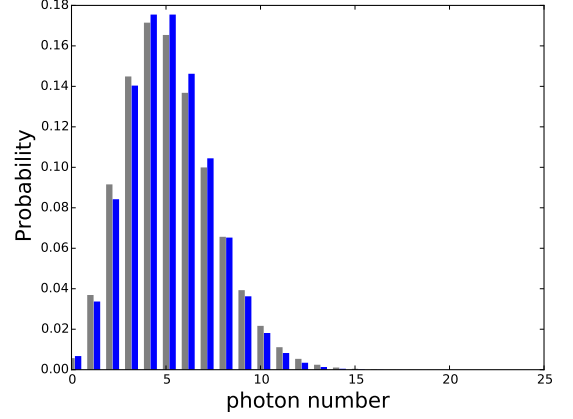


FIG. 3: (Color Online) EM reconstruction of photon number statistics from a sequence of simulated homodyne measurements for a coherent state. The blue histogram bars represent a true photon distribution. The gray histogram bars correspond to a distribution reconstructed by using the EM algorithm.

To illustrate our EM-based photon number statistics inference scheme we applied it to a sequence of 32768 simulated homodyne measurement outcomes for a coherent state $\rho = |\alpha\rangle\langle\alpha|$ with the mean photon number $|\alpha|^2 = 5$. To reconstruct the photon number statistics from the simulated measurement data, we have selected a mixture model with $N_{max} = 20$ (21-component model). The results of EM reconstruction (after 9 iterations) are plotted on Fig.(3) and demonstrate a good quantitative agreement with the true state.

III. EXPERIMENTS

We apply the theory developed in Sec.II in experiments to reconstruct photon number distributions of a weak coherent state and a thermal state.

A. Detector efficiency

In Sec.II, we have assumed perfect homodyne detectors with unity efficiency. Here we consider practical detector with non-unity detection efficiency. It is well known that a realistic photo-detector with efficiency η can be modeled by placing a virtual beam splitter (with a transmittance of η) in front of an ideal detector [25]. By assuming the four photo-detectors have identical efficiency, we can model the conjugate homodyne detection using the setup shown in Fig.4(a). In Appendix A we will show that given the LOs are strong enough, Fig.4(a) is equivalent to Fig.4(b), where the four virtual beam splitters in front of the photo-detectors are replaced by a common virtual beam splitter (with the same transmittance) at

the input path of the first beam splitter. This is very convenient in practice since we can apply the theory in Sect. II directly to the experimental results by assuming the photo-detectors are ideal. The photon number distribution reconstructed this way is related to that of the input state by the Bernoulli transformation [26]. By further applying the inverse Bernoulli transformation, the photon number distribution of the input state can be determined.

In our experiments, either a weak coherent source or a thermal source is employed as the input. In this case, the state after the virtual beam splitter in Fig.4(b) is still a coherent state (or a thermal state) with a reduced average photon number. We simply redefine the state after the virtual beam splitter as the input state and compare its photon number distribution with the one reconstructed experimentally.

B. Experimental setup

The experimental setup is shown in Fig.5. A continuous wave (CW) laser at telecom wavelength (Clarity-NLL-1542-HP from Wavelength Reference) is employed as the LO. The conjugate optical homodyne detection system is constructed by a commercial 90° optical hybrid (Optoplex) and two 350 MHz balanced amplified photodetectors (Thorlabs). The 90° optical hybrid is essentially a six-port interferometer with four beam splitters inside: three as shown in Fig.1 and another one for generating two conjugate LOs from a common one. It is a passive device featuring a compact design and no temperature control is required for phase stabilization. Variable optical attenuators are used to balance the detection efficiency of different channels and control the average photon number of the input state. The outputs of the two balanced photodetectors are sampled by a two-channel data acquisition board (Texas Instruments).

C. Experimental results

For simplicity, both the LO laser and the photon source under test are operated in a CW mode. In the first experiment, a heavily attenuated laser source is used to provide a weak coherent state input. By adjusting the variable optical attenuator, the average photon number within one sampling window has been set to 5 (after correction of detection efficiency). In the second experiment, an amplified spontaneous emission (ASE) source is used to provide a thermal state input (with an average photon number of 15.3). Note, while the output of the ASE source contains multiple modes, the homodyne detector selectively measures the one matched with the LO mode. Limited by the memory size of the data acquisition board, 32728 quadrature pairs are sampled in each measurement.

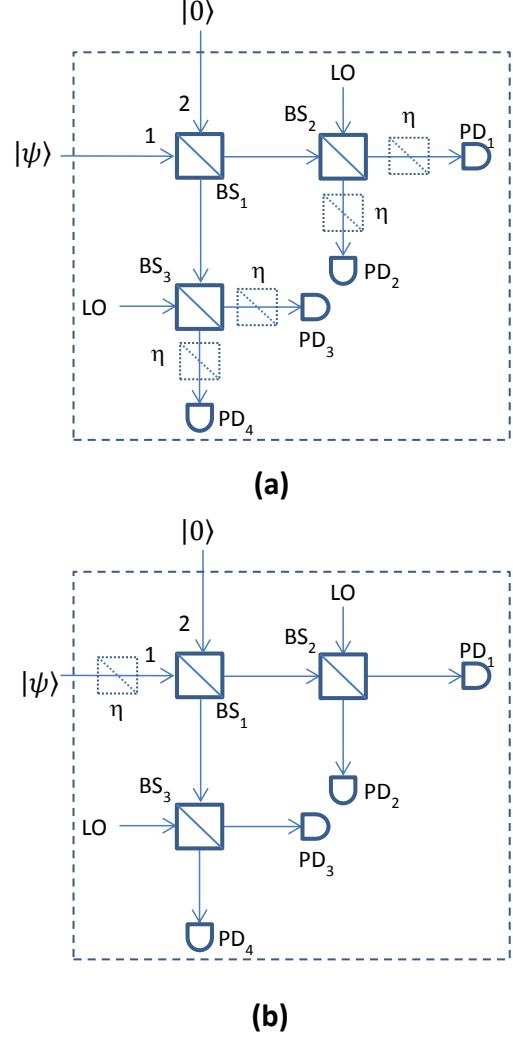


FIG. 4: Models of realistic photo-detector with detection efficiency η . (a) The actual setup. (b) An equivalent model of (a). See details in Appendix A.

Using Eq.(1), we calculate the parameter z from the quadrature measurement results. Using Eq.(15), we determined the $g^{(2)}(0)$ factors of the two sources to be 1.11 (weak coherent source) and 1.94 (thermal source) correspondingly. The deviation from the ideal values of 1 (coherent state) and 2 (thermal state) are likely due to the detector noise and imperfection of source.

Next we apply the EM algorithm described in details in Section II C to the experimental data in order to reconstruct the photon number statistics of various light sources. In Fig. 6 we plot reconstruction results for a weak coherent state. The blue bars represent the photon number statistic of a coherent state $|\alpha\rangle$ with the mean number of photons $|\alpha|^2 = 5$, assuming noiseless detectors. The red bars correspond to the numerically synthesized data from the coherent state $|\alpha\rangle$ with added Gaus-

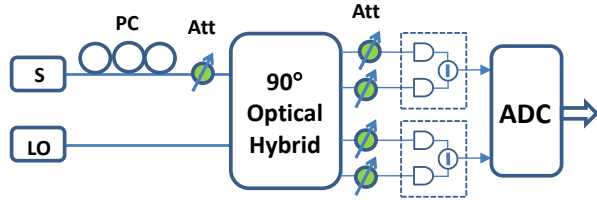


FIG. 5: Experimental setup. S-photon source under test; LO-local oscillator; PC-polarization controller; Att-variable optical attenuator; ADC-data acquisition board.

sian noise which mimics the effect of noisy photo detectors. We assume that the noise has zero mean and variances $\sigma_{X_3}^2 = 0.21, \sigma_{P_4}^2 = 0.16$ for the quadratures X_3 and P_4 respectively which are the actual values measured in our experiments. The green bars depict the photon number statistics obtained from raw experimental data by using the EM algorithm. We note that the red and green histograms look remarkably similar which implies that experimental data come from a coherent state affected by the detector noise. In Fig. 7 we depict EM reconstruction results for a thermal state with the mean photon number $\bar{n}_{th} = 15.3$. The black bars represent the photon number statistics of a thermal state with $\bar{n}_{th} = 15.3$. The red bar are EM reconstruction results using numerically simulated quadrature measurement data with added detector noise. Like in the case of the coherent state, we assume that the detector noise is Gaussian with zero mean and variances $\sigma_{X_3}^2 = 0.21, \sigma_{P_4}^2 = 0.16$. Finally, the blue bars correspond to EM reconstruction of actual experimental data. We notice that for the thermal state the three distributions are very close visually. This is because the detector noise is much smaller than the mean number of photons in the state. Therefore, the noise effects are not as pronounced as in the case on a weak coherent state in Fig. 6.

IV. DISCUSSION

Classically, the intensity of a single-mode light pulse can be determined by measuring two conjugate quadratures simultaneously. Quantum mechanically, the above measurement process is intrinsically noisy. In this paper, we develop theoretical tools to reconstruct photon number statistics of a single-mode quantum state by performing conjugate homodyne detection. Comparing with previous studies based on single homodyne detection, no LO phase randomization is required in our scheme. This simplifies its implementation. We further apply the above theoretical results to determine the photon number statistic of a weak coherent state and a thermal state.

We acknowledge helpful comments from Ryan S. Ben-

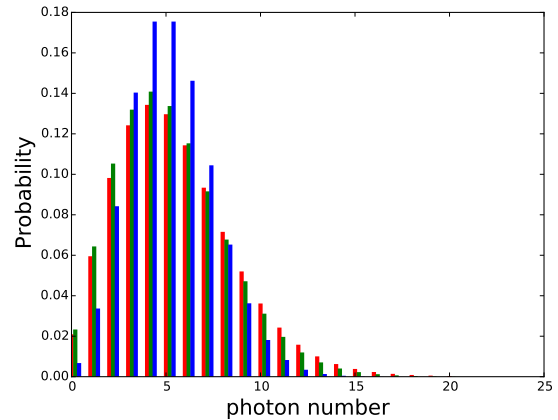


FIG. 6: (Color Online) Histograms of the reconstructed photon number distributions for a coherent state $|\alpha\rangle$: a) Photon number statistics for $|\alpha|^2 = 5$ (blue) b) Simulated measurement for $|\alpha|^2 = 5$ data with added detector noise (red) c) Experimental data (green).

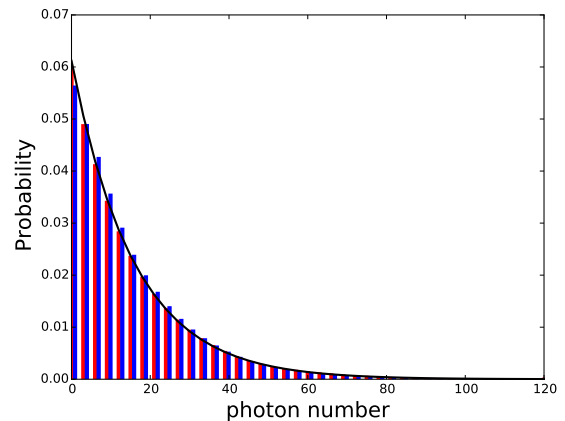


FIG. 7: (Color Online) Histograms of the reconstructed photon number distributions for a thermal state with the mean photon number = 15.3: a) Simulated measurement data with added detector noise (red) b) Reconstruction results for experimental data (blue) c) Thermal distribution with the mean photon number = 15.3 (black).

nink, Warren Grice, Charles C. W. Lim and Nicholas A. Peters. This work was performed at Oak Ridge National Laboratory (ORNL), operated by UT-Battelle for the U.S. Department of Energy under Contract No. DE-AC05-00OR22725. The authors acknowledge support from ORNL laboratory directed research and development program.

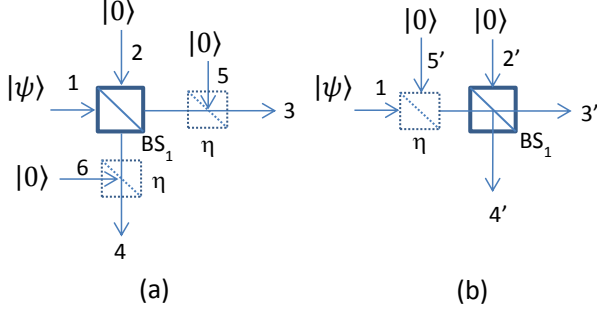


FIG. 8: Two equivalent models. (a) A symmetric beam splitter followed by two virtual beam splitters. (b) A virtual beam splitter placed in front of the symmetric beam splitter.

Appendix A: Detector efficiency in the conjugate homodyne scheme

In this Appendix, we will show that given the LOs are strong enough, the setup shown in Fig.4(a) is equivalent to that in Fig.4(b), where the four virtual beam splitters in front of the photo-detectors are replaced by a common virtual beam splitter (with the same transmittance) at the input path of the first beam splitter.

Given the LO is strong enough, a single DC-balanced homodyne detector using two realistic (non-unity efficiency) and identical photo-detectors can be modeled by the one with ideal photo-detectors by placing a virtual beam splitter at the signal input [27]. This allows us to replace the four virtual beam splitters in Fig.4(a) by two virtual beam splitters with the same transmittance (one at each of the output port of the first beam splitter). We will show that these two virtual beam splitters can be further replaced by one as shown in Fig.4(b). More specifically, we will show the two models in Fig.8 are equivalent to each other.

For simplicity, we define the transmittance of the virtual beam splitter as $\eta = \cos \gamma$.

From Fig.8(a) and using the transmission relations of lossless beam splitter, we have

$$\begin{aligned}\hat{X}_3 &= \frac{1}{\sqrt{2}} \cos \gamma \hat{X}_1 + \frac{1}{\sqrt{2}} \cos \gamma \hat{X}_2 + \sin \gamma \hat{X}_5 \\ &= \frac{1}{\sqrt{2}} \cos \gamma \hat{X}_1 + \frac{1}{\sqrt{2}} \sqrt{1 + \sin^2 \gamma} \hat{X}_{V1}\end{aligned}\quad (\text{A1})$$

where $\hat{X}_{V1} = \frac{\cos \gamma}{\sqrt{1 + \sin^2 \gamma}} \hat{X}_2 + \frac{\sqrt{2} \sin \gamma}{\sqrt{1 + \sin^2 \gamma}} \hat{X}_5$. Since the inputs of mode 2 and mode 5 in Fig.8(a) are vacuum, the unitary transformation described above yields another vacuum state. So \hat{X}_{V1} at the RHS of (A1) can be interpreted as the X-quadrature of vacuum state.

Similarly, the P-quadrature of mode 4 in Fig.8(a) is given by

$$\begin{aligned}\hat{P}_4 &= \frac{1}{\sqrt{2}} \cos \gamma \hat{P}_1 - \frac{1}{\sqrt{2}} \cos \gamma \hat{P}_2 + \sin \gamma \hat{P}_5 \\ &= \frac{1}{\sqrt{2}} \cos \gamma \hat{P}_1 + \frac{1}{\sqrt{2}} \sqrt{1 + \sin^2 \gamma} \hat{P}_{V2}\end{aligned}\quad (\text{A2})$$

$$\text{where } \hat{P}_{V2} = -\frac{\cos \gamma}{\sqrt{1 + \sin^2 \gamma}} \hat{P}_2 + \frac{\sqrt{2} \sin \gamma}{\sqrt{1 + \sin^2 \gamma}} \hat{P}_5.$$

We can apply the same process in the model shown in Fig.8(b) and have the following relations:

$$\begin{aligned}\hat{X}_{3'} &= \frac{1}{\sqrt{2}} \cos \gamma \hat{X}_1 + \frac{1}{\sqrt{2}} \sin \gamma \hat{X}_{5'} + \frac{1}{\sqrt{2}} \hat{X}_{2'} \\ &= \frac{1}{\sqrt{2}} \cos \gamma \hat{X}_1 + \frac{1}{\sqrt{2}} \sqrt{1 + \sin^2 \gamma} \hat{X}_{V3}\end{aligned}\quad (\text{A3})$$

$$\text{where } \hat{X}_{V3} = \frac{\sin \gamma}{\sqrt{1 + \sin^2 \gamma}} \hat{X}_{5'} + \frac{1}{\sqrt{1 + \sin^2 \gamma}} \hat{X}_{2'}$$

$$\begin{aligned}\hat{P}_{4'} &= \frac{1}{\sqrt{2}} \cos \gamma \hat{P}_1 + \frac{1}{\sqrt{2}} \sin \gamma \hat{P}_{5'} - \frac{1}{\sqrt{2}} \hat{P}_{2'} \\ &= \frac{1}{\sqrt{2}} \cos \gamma \hat{P}_1 + \frac{1}{\sqrt{2}} \sqrt{1 + \sin^2 \gamma} \hat{P}_{V4}\end{aligned}\quad (\text{A4})$$

$$\text{where } \hat{P}_{V4} = \frac{\sin \gamma}{\sqrt{1 + \sin^2 \gamma}} \hat{P}_{5'} - \frac{1}{\sqrt{1 + \sin^2 \gamma}} \hat{P}_{2'}.$$

It is easy to show X_{V1} , P_{V2} , X_{V3} , P_{V4} are independent and identically distributed random variables. From (A1)-(A4), the joint probability of X_3 and P_4 is the same as that of $X_{3'}$ and $P_{4'}$. So the two models given in Fig.8 are equivalent.

-
- [1] R. H. Hadfield, *Nature Photonics* **3**, 696 (2009).
 - [2] K. Vogel and H. Risken, *Phys. Rev. A* **40**, 2847 (1989).
 - [3] A. I. Lvovsky and M. G. Raymer, *Rev. Mod. Phys.* **81**, 299 (2009).
 - [4] N. Gisin, G. Ribordy, W. Tittel, and H. Zbinden, *Rev. Mod. Phys.* **74**, 145 (2002).

- [5] V. Scarani, H. Bechmann-Pasquinucci, N. J. Cerf, M. Dušek, N. Lütkenhaus, and M. Peev, *Rev. Mod. Phys.* **81**, 1301 (2009).
- [6] H.-K. Lo, M. Curty, and K. Tamaki, *Nature Photonics* **8**, 595 (2014).
- [7] E. Diamanti, H.-K. Lo, B. Qi, and Z. Yuan, *npj Quantum*

- Information* **2**, 16025 (2016).
- [8] B. Qi, W. Zhu, L. Qian, and H.-K. Lo, *New J. Phys.* **12**, 103042 (2010).
 - [9] R. Kumar, H. Qin, and R. Alléaume, *New J. Phys.* **17**, 043027 (2015).
 - [10] B. Heim, C. Peuntinger, N. Killoran, I. Khan, C. Wittmann, Ch. Marquardt, and G. Leuchs, *New J. Phys.* **16**, 113018 (2014).
 - [11] H. P. Yuen and V. W. S. Chan, *Opt. Lett.* **8**, 177 (1983).
 - [12] G. L. Abbas, V. W. S. Chan, and T. K. Yee, *Opt. Lett.* **8**, 419 (1983).
 - [13] M. Munroe, D. Boggavarapu, M. E. Anderson, and M. G. Raymer, *Phys. Rev. A* **52**, R924 (1995).
 - [14] S. Schiller, G. Breitenbach, S. F. Pereira, T. Müller, and J. Mlynek, *Phys. Rev. Lett.* **77**, 2933 (1996).
 - [15] U. Leonhardt, M. Munroe, T. Kiss, Th. Richter, and M. G. Raymer, *Opt. Commun.* **127**, 144 (1996).
 - [16] Th. Richter, *J. Mod. Opt.* **45**, 1735 (1998).
 - [17] Y. Zhao, B. Qi, and H.-K. Lo, *Appl. Phys. Lett.* **90**, 044106 (2007).
 - [18] R. Loudon, *The Quantum Theory of Light* (Oxford University Press, Oxford, England, 2000).
 - [19] We could remove the constant 1 by redefining Eq. (1) as $z = x_3^2 + p_4^2 - 1$. However, the revised definition may result a negative measurement result of Z in a single-shot measurement.
 - [20] R. J. Glauber, *Phys. Rev.* **130**, 2529 (1963).
 - [21] G. Roumpos and S. T. Cundiff, *Opt. Lett.* **38**, 139 (2013).
 - [22] W. Grice and I. A. Walmsley, *J. Mod. Opt.* **43**, 795 (1996).
 - [23] A. P. Dempster, N. M. Laird and D. B. Rubin, *Journal of the Royal Statistical Society. Series B (Methodological)* **39**, pp. 1-38 (1977).
 - [24] K. Banaszek, *Phys. Rev. A* **57**, 5013 (1998).
 - [25] H. P. Yuen and J. H. Shapiro, in *Coherence and Quantum Optics IV*, edited by L. Mandel and E. Wolf (Plenum, New York, 1978), p. 719.
 - [26] C. T. Lee, *Phys. Rev. A* **48**, 2285 (1993).
 - [27] U. Leonhardt and H. Paul, *Phys. Rev. A* **48**, 4598 (1993).